ARTICLE

Check for updates

Conditions for walk-off soliton generation in a multimode fiber

Mario Zitelli[1 ✉], Fabio Mangini [2], Mario Ferraro [1], Oleg Sidelnikov[3] & Stefan Wabnitz[1,3]

It has been recently demonstrated that multimode solitons are unstable objects which evolve, in the range of hundreds of nonlinearity lengths, into stable single-mode solitons carried by the fundamental mode. We show experimentally and by numerical simulations that femto-second multimode solitons composed by non-degenerate modes have unique properties: when propagating in graded-index fibers, their pulsewidth and energy do not depend on the input pulsewidth, but only on input coupling conditions and linear dispersive properties of the fiber, hence on their wavelength. Because of these properties, spatiotemporal solitons composed by non-degenerate modes with pulsewidths longer than a few hundreds of fem-toseconds cannot be generated in graded-index fibers.

[1] Department of Information Engineering, Electronics and Telecommunications (DIET), Sapienza University of Rome, Rome, Italy. [2] Department of Information Engineering (DII), University of Brescia, Brescia, Italy. [3] Novosibirsk State University, Novosibirsk, Russia. ✉email: mario.zitelli@uniroma1.it

Pioneering works on multimode (MM) fiber transmission[1,2], dated 40 years ago, predicted the existence of MM solitons, providing conditions for the temporal trapping of the input optical modes, in order to form a MM or spatiotemporal soliton[3,4]. Research on multimode fibers (MMFs) is a topic of renewed interest, motivated by their potential for increasing the transmission capacity of long-distance optical fiber transmissions via the mode-division-multiplexing technique, based on multiple spatial modes as information carriers. Moreover, the capacity of MMFs to carry high-energy beams permits the upscaling of high-power fiber lasers. However, MM fiber solitons have only recently been systematically experimentally investigated in graded-index (GRIN) MMFs, unveiling the complexity of a new, previously uncharted field[5–11]. For example, ref. [9] has shown that the spatiotemporal oscillations of solitons, due to self-imaging in a GRIN fiber, generate MM dispersive waves over an ultrabroadband spectral range, leading to a new source of coherent light with unprecedented spectral range. Moreover, in ref. [10], a study of the fission of high-order MM solitons has revealed that the generated fundamental solitons have a nearly constant Raman wavelength shift and equal pulsewidth over a wide range of soliton energies. In a recent study[11], we observed that the beam content of femtosecond MM solitons propagating over relatively long spans of GRIN fiber is irreversibly attracted toward the fundamental mode of the MMF. This is due to the combined action of inter-modal four-wave mixing (IM-FWM) and stimulated Raman scattering (SRS).

In this work, we extensively study the dynamics of the generation of these femtosecond MM soliton beams. We reveal the existence of previously unexpected dynamics, which make these MM solitons very different from their well-known single-mode counterparts. In single-mode fibers, a soliton forms when chromatic dispersion pulse broadening is compensated for by self-phase modulation-induced pulse compression. Specifically, the nonlinear and the chromatic dispersion distances must be equal. This means that a single-mode soliton can have an arbitrary temporal duration, provided that its peak power or energy is properly adjusted. In contrast, for obtaining a MM soliton in a MMF, it is additionally required to compensate for modal dispersion or temporal walk-off. As a result, it is necessary to impose the additional condition that the walk-off distance is of the same order of the nonlinear and chromatic dispersion lengths. The presence of this extra condition leads to a new class, to the best of our knowledge, of "walk-off" MM solitons composed of non-degenerate modes: they have a pulsewidth and energy, which are independent of the input pulse duration, and only depend on the fiber dispersive parameters, hence the soliton wavelength.

Results

Experimental evidence. The transmission of ultrashort pulses (input pulsewidth and wavelength were 60–240 fs, and 1300–1700 nm, respectively) was tested over long spans of graded-index (GRIN) optical fiber (see "Methods"—"Experiments"). When coupling exactly on the fiber axis, with 15 μm input beam waist, we could excite three nondegenerate, axial-symmetric Laguerre–Gauss modes, that will be addressed from now on as (0,0), (1,0), (2,0) or LG_{01}, LG_{02}, LG_{03}. The fraction of power carried by these modes was calculated by a specific software (see[12] and Supplementary note 1) to be 52%, 30%, and 18%, respectively. The input laser pulse energy ranged between 0.1 and 20 nJ.

What we observed did not appear to obey the predictions of the variational theory for spatiotemporal solitons[13–18]: Figs. 1–3 provide the experimental evidence when using 120 m of GRIN fiber. By testing different input wavelengths (1420–1550 nm) and input pulsewidths (67–245 fs), spatiotemporal solitons with a
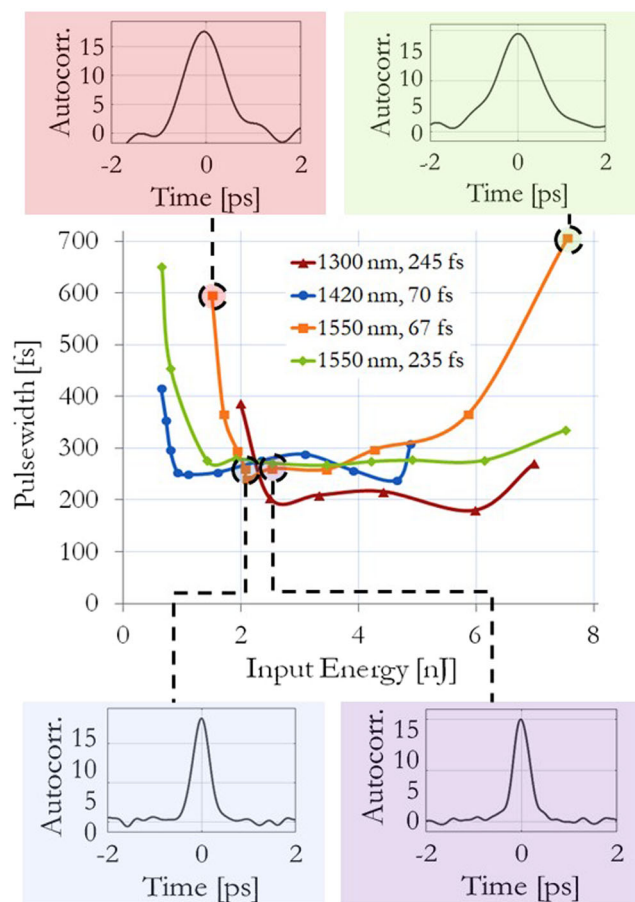

Fig. 1 Measured soliton pulsewidth vs. input pulse energy, after 120 m of graded-index (GRIN) fiber, for different input wavelengths and pulse durations. The insets are the measured output autocorrelation traces, for an input wavelength 1550 nm and pulsewidth 67 fs. Measurement error comes directly from the instrument accuracy, that is below 1%, i.e., too small to be visible at this scale.

common minimum pulsewidth of 260 fs were observed at the fiber output, for values of the input pulse energy ranging from 2 up to 4 nJ (Fig. 1). The case of a 1300 nm input wavelength represented an exception, which resulted into a minimum pulsewidth of 200 fs at higher energies.

The output beam waist (Fig. 2) was severely reduced from its input value (down to a value of 8.5 μm, which is close to the theoretical value of 7.7 μm for the fundamental fiber mode), in correspondence of the input energy leading to minimum output pulsewidth. In this regime, the output beam shape was substantially monomodal, with a measured $M^2 = 1.45$, against the value of 1.3 of the input beam. The curve of the beam waist vs. energy was much narrower for input short (67 fs) pulses than for long (235 fs) pulses; also for the beam waist, the case of 1300 nm represented an exception, with no significant beam reduction. The output soliton wavelength (Fig. 3) was severely affected by Raman soliton self-frequency shift (SSFS)[3,7]. Still, the case of 1300 nm represented an exception, that provided reduced values of SSFS.

The explanation to the relatively sharp dependence of the output beam diameter on the input pulse energy in Fig. 2, for 67 fs pulses, is found in linear fiber losses and wavelength red-shift. As a matter of fact, shorter pulses suffer faster soliton SSFS for increasing energy, and experience increased linear fiber losses when the wavelength overcomes 1700 nm[11](Figs. 1 and 3). As a result, while the propagating soliton is attenuated, dispersive waves provide a more significant relative contribution to the
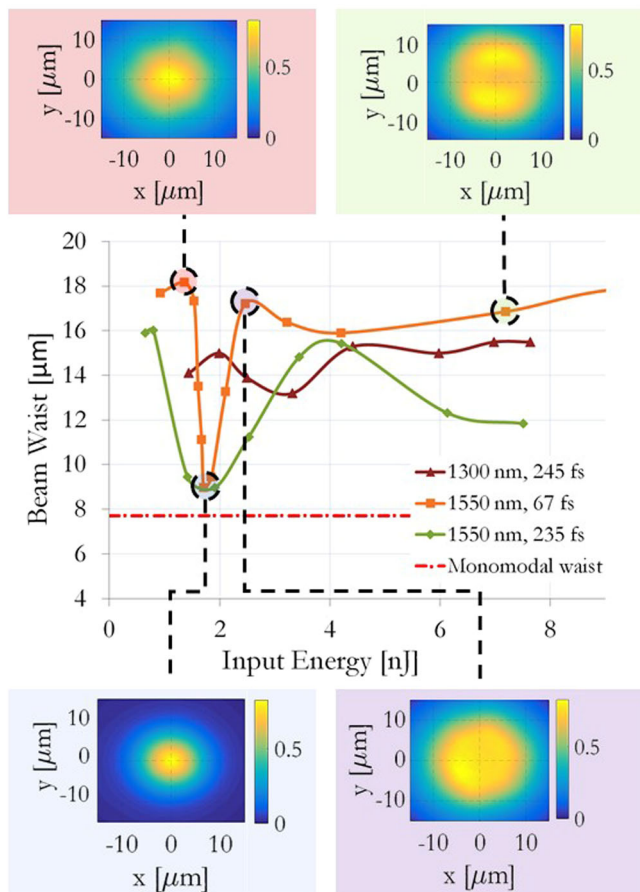
Fig. 2 Measured soliton beam waist vs. input pulse energy, after 120 m of graded-index (GRIN), in the same conditions of Fig. 1. The insets show the measured output near-fields, for an input wavelength 1550 nm and pulsewidth 67 fs. Infrared (IR) camera resolution is 0.25 μm, which is too small to be visible at this scale.

Fig. 3 Measured soliton wavelength vs. input pulse energy, after 120 m of graded-index (GRIN) fiber, in the cases of Fig. 1. The insets show the measured output spectra, for an input wavelength 1550 nm and pulsewidth 67 fs. Spectrometer resolution is 0.2 nm, which is too small to be visible at this scale.

output beam image, which integrates energy over all wavelengths within the camera response window. On the other hand, longer pulses suffer a slower SSFS, as seen when comparing, in Fig. 3, cases at 1550 nm and 235 or 67 fs input pulsewidth. Therefore, the output beam waist reduction or beam cleaning process appears smoother when the input energy changes. The same considerations also apply to the fundamental beam waist itself, $w_e = (\lambda r_c / \sqrt{2\Delta} \pi n_{\mathrm{eff}})^{1/2}$, being λ the wavelength, r_c the core radius, Δ the relative index difference, and n_{eff} the modal index; the waist scales with the square root of the increasing wavelength, resulting in a broadened fundamental beam at the fiber output. In addition, it should be considered that the response of the InGaAs camera used in our experiments sharply drops for wavelengths above 1850 nm, which impairs its ability to record the red-shifting soliton above this wavelength.

In all cases, numerical simulations performed with a coupled-mode equations model (see "Methods"—"Simulations") fully confirmed the experimental results (empty dots).

Experimental evidence with either shorter or longer spans of GRIN fiber, ranging from 2 to 850 m (Fig. 4), shows that requirements for the optimal soliton energy as the fiber length is reduced are less stringent. At 850 m distance, 1550 nm and 67 fs input pulsewidth, a sharp input energy of 1.5 nJ is required to obtain a minimum pulsewidth of 470 fs at output; at 120 m, a minimum pulsewidth of 260 fs is measured for energy range between 2 and 4 nJ; at 10 and 2 m distance, pulsewidth remains minimum (110 and
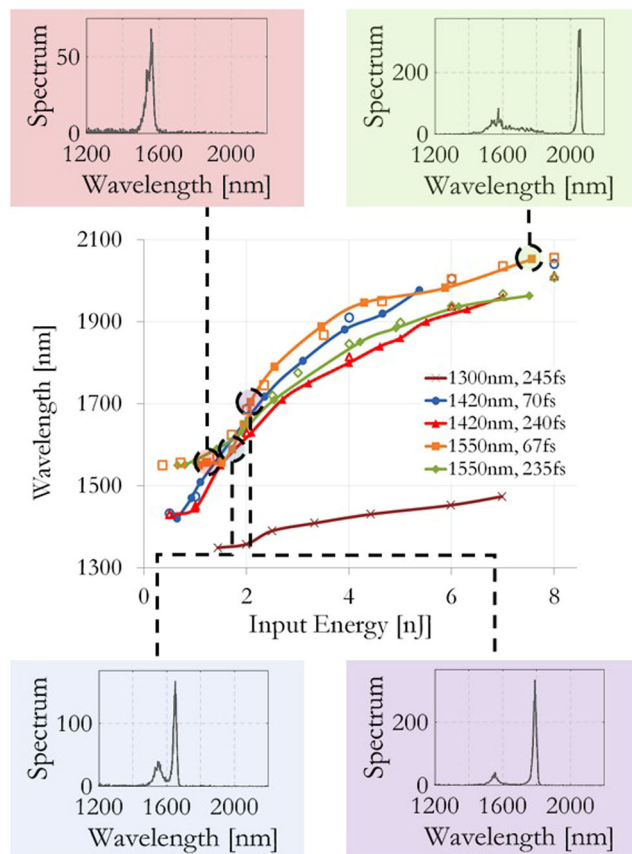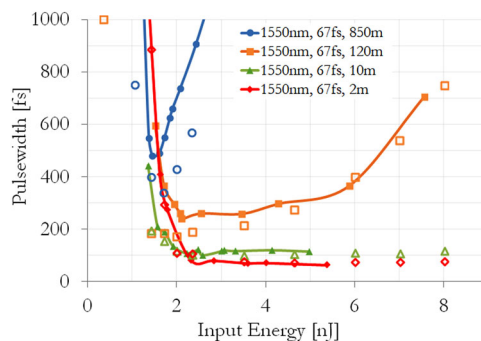

Fig. 4 Measured soliton pulsewidth vs. input energy, for input pulses with 1550 nm wavelength, 67 fs pulsewidth, and 15 μm input waist, respectively, with graded-index (GRIN) fiber spans of length 2, 10, 120, and 850 m. Measurement error comes directly from the instrument accuracy, that is below 1%, too small to be visible at this scale.

60 fs, respectively), for input energies larger than 2.5 nJ. Soliton pulsewidth increases with distance, as a consequence of the wavelength red-shift due to Raman SSFS, and the need to conserve the soliton energy condition $E_1 = \lambda |\beta_2(\lambda)| w_e^2 / n_2 T_0$, with $T_0 = T_{\mathrm{FWHM}}/1.763$, $n_2 (m^2 W^{-1})$ the nonlinear index coefficient, $\beta_2(\lambda)$ the chromatic dispersion, and w_e the effective beam waist.

Note that the "sharp" resonance for 67 fs input temporal duration at 1550 nm is not seen in Figs. 1 and 3, because with the
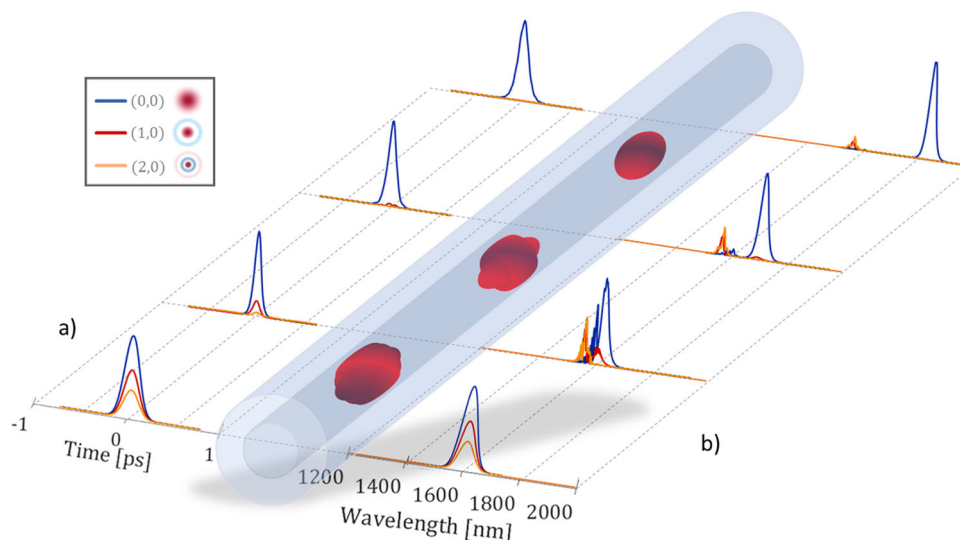
Fig. 5 Spatiotemporal soliton formed from an input 235 fs pulse. The soliton is composed by three axial modes, propagating over 120 m of graded-index (GRIN) fiber, for the optimal input energy of 2.5 nJ. (a) modes power, (b) modes spectra.

autocorrelator and the optical spectrum analyzer, one directly monitors the pulse duration and the wavelength of the Raman soliton, even if its relative amplitude drops with respect to the residual dispersive waves remaining around 1550 nm. Numerical simulations (empty dots) substantially confirmed the experimental observations. In our experiments, the minimum output pulsewidth, at 120 m distance, appeared to be independent of the input pulsewidth and wavelength, and it was obtained at comparable input energies in all cases. The case at 1300 nm showed a different behavior. We started investigating our observations from numerical simulations.

Numerical simulations. Figure 5 provides an explanation to the observed spatiotemporal effects; it is a numerical representation of the evolution of an input 235 fs pulse, composed of three axial modes, propagating over 120 m of GRIN fiber, at the optimal input energy of 2.5 nJ. During their propagation, the three nondegenerate modes remain temporally trapped; the mode LG_{01} acts as an attractor for other modes, owing to non-phase matched, asymmetrical IM-FWM, and to intermodal SRS[11]; at the output, a monomodal bullet remains. The pulse carried by the fundamental or LG_{01} mode experiences SSFS, while it traps and captures a large portion of energy carried by higher-order modes. The observed process of spatial beam cleaning becomes more efficient when the soliton wavelength shift reaches roughly 100 nm with respect to the residual dispersive wave; it is therefore principally a Raman beam cleanup process, but not of a pump-probe type as discussed in ref. [19] because the pump and the Stokes probe are indeed co-propagating within the spectrum of the same soliton pulse, and the residual dispersive wave may become negligible in some conditions.

In order to explain the observed temporal effects, we present in Fig. 6 numerical simulation results that shed light on the process of soliton formation. Figure 6a compares the evolution of the temporal duration of pulses launched with either 67 or 235 fs input pulsewidth, for different input wavelengths (1350, 1550, or 1680 nm). In each case, we picked the optimal input energy that produces a minimum pulsewidth at 120 m. Input energies range between 2 and 3 nJ when going from shorter to longer wavelengths, and remain the same for both initial pulsewidths of 67 or 235 fs, respectively. Input pulses with the same wavelength and different durations always form a soliton with identical pulsewidth T_{s0}. The necessary propagation distance for soliton formation is 1 m at
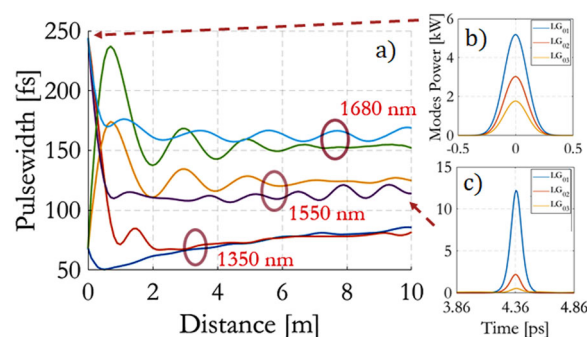

Fig. 6 Evolution with fiber length of simulated soliton pulsewidths for different input pulse durations and wavelengths. Simulations for input pulses of 67 and 235 fs duration, and wavelengths of 1350, 1550, 1680 nm, respectively (**a**). The input modes are LG_{01}, LG_{02}, LG_{03}. Modal powers at the fiber input (**b**), and after 10 m of propagation (**c**), for input 1550 nm input wavelength and 235 fs input pulsewidth.

1350 nm, and 6 m for both 1550 and 1680 nm. As the soliton propagates, its pulsewidth grows larger because of SSFS, which increases its wavelength, and local fiber dispersion, so that the soliton condition is maintained[10,20,21]. For longer distances, the pulsewidth differences, which are observed in Fig. 6a for different input wavelengths, approach to a common value, as experimentally confirmed at 120 m (see Fig. 2). Correspondingly, one observes a redistribution of the input modal powers (Fig. 6b) toward the fundamental mode of the GRIN fiber, as in the example of Fig. 6c, which is obtained after 10 m of propagation.

Discussion

All input pulses with the same wavelength, comparable energies, and different pulsewidths, generated after a few meters of propagation a spatiotemporal soliton with common pulsewidth T_{s0}. T_{s0} increased for growing values of the input wavelength. Once that the spatiotemporal soliton was formed, a slow energy transfer into the LG_{01} mode was experimentally observed, while the soliton simultaneously experiences SSFS (Fig. 3). For distances larger than 100 m, the generated soliton appeared to be intrinsically monomodal, with a near-field waist approaching that of the fundamental mode of the MMF (Fig. 2). For all tested wavelengths and pulsewidths, a long-distance soliton was always

observed for comparable input energies (i.e., between 2 and 3 nJ in the case of initial excitation of three axial modes). Numerical simulations (See Fig. 1 in Supplementary note 2) and experiments[11] confirmed that similar monomodal solitons are observed when launching a larger number of degenerate and nondegenerate modes at the fiber input, by varying the input beam size or angle.

A possible analytical explanation for the invariance of the observed pulsewidth T_{s0} of the generated solitons is provided considering the modal walk-off length. From numerical simulations, we know the wavelength dependence of the fiber dispersion parameters of different fiber modes. Specifically, we know the group velocities, say, $\beta_{11}(\lambda)$, $\beta_{12}(\lambda)$, $\beta_{13}(\lambda)$ (ps km^{-1}) for the three axial modes LG$_{01}$, LG$_{02}$, LG$_{03}$, as well as their group velocity dispersion $\beta_2(\lambda)$ (ps^2 km^{-1}), which can be assumed to be equal for all of the three modes. The resulting weighted mean of the group velocity difference can be written as: $\overline{\Delta\beta_1} = \left[0.30\left(\beta_{12}(\lambda) - \beta_{11}(\lambda)\right) + 0.18\left(\beta_{13}(\lambda) - \beta_{11}(\lambda)\right)\right]/(0.30 + 0.18)$.

Let us recall now the following characteristic lengths: the mean modal walk-off length of the forming soliton $L_W = T_0/\overline{\Delta\beta_1}$, with $T_0 = T_{s0}/1.763$, is defined as the distance where, in the linear regime, the modes separate temporally. The pulse nonlinearity length L_{NL} and its dispersion length $L_D = T_0^2/\left|\beta_2(\lambda)\right|$, are defined as the characteristic length scales for Kerr nonlinearity and chromatic dispersion, respectively. The random mode coupling and birefringence correlation lengths, L_{cm} and L_{cp}, are the characteristic length scales associated with linear coupling between degenerate modes or between polarizations, respectively[22–24].

In order to explain our observations, we may assume that, when nonlinearity acts over distances shorter than those associated with random mode coupling and birefringence, i.e., for $L_{NL} < L_{cm}, L_{cp}$, it is possible to observe a spatiotemporal soliton, which is attracted into an effectively single-mode soliton[11]. A second requirement to be considered is that both of the dispersion and nonlinearity lengths are comparable with the fiber walk-off length: $L_D = L_{NL} = \text{const} \cdot L_W$, being const an adjustment constant close to one. A similar condition for temporal trapping of the optical modes was initially predicted, for the jth mode, by refs. [1,2] as $L_{Wj} \geq L_D = L_{NL}$.

Based on the above considerations, we may find the condition to be respected by the soliton pulsewidth at the distance of initial formation

$$T_{S0}(\lambda) = \text{const} \cdot 1.763 \frac{\left|\beta_2(\lambda)\right|}{\Delta\beta_1(\lambda)} \tag{1}$$

By performing a cut-back experiment, we measured the forming soliton pulsewidth at 1 m of distance (at 1300, 1350, and 1420 nm) and at 6 m of distance (at 1550, 1680 nm), for the optimal input energies of 2–3 nJ, and input pulsewidths ranging between 61 and 96 fs (depending on the input wavelength). We compared experimental results with numerical simulations at different input wavelengths and input pulsewidths of 67 and 235 fs, and with the theoretical curve of T_{s0} upon wavelength as it is obtained from Eq. (1), by using the dispersion curves of a GRIN fiber. The corresponding results are shown in Fig. 7, confirming the good agreement between theory and experiments/simulations, provided the adjustment constant is set to const = 0.87, and for wavelengths above 1350 nm (the const value may change with the coupling conditions). Whereas for wavelengths below 1350 nm, the (anomalous) dispersion becomes very small, and the theory fails in predicting solitons with unphysical short pulse durations, also because we neglect the presence of higher-order dispersion terms.

Therefore, Eq. (1) confirms that a spatiotemporal soliton, including nondegenerate modes, may be formed from the initial pulse, eventually leaving behind a certain amount of energy in dispersive
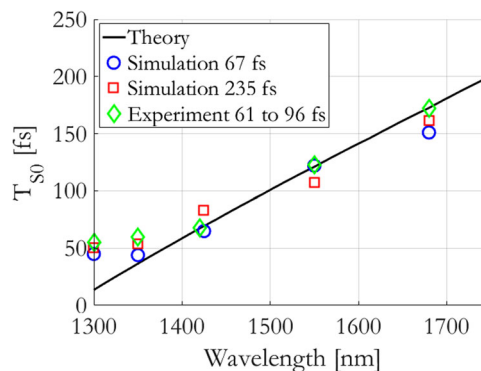

Fig. 7 Theoretical curve of soliton pulse duration vs. wavelength, compared with measured and simulated soliton pulsewidth. Experiments carried out with 1 m of graded-index (GRIN) fiber, with input wavelength and pulsewidth: 1300 nm and 61 fs, 1350 nm and 61 fs, or 1420 nm and 70 fs, respectively. Experiment carried out with 6 m of GRIN fiber, with input wavelength and pulsewidth: 1550 nm and 67 fs, 1680 nm and 96 fs, respectively. Measurement error comes directly from the instrument accuracy, which is below 1%. Simulations were carried out with same distances and input wavelengths as in the experiments, with pulsewidths of 67 and 235 fs, respectively.

waves. The soliton initial pulsewidth, and therefore energy, depends on the fiber dispersion parameters. Our solitonic object appears to be clamped to the fiber walk-off length L_W, in the sense that the walk-off, dispersion, and nonlinearity lengths must be related by an exact equation, with const dependent on the MM soliton modal distribution. The soliton pulsewidth T_{s0}, at its formation distance, varies with the wavelength of the input pump pulse, but its value turns out to be independent of input pulse duration. From Fig. 7, we find that a soliton with a duration longer than a few hundreds of femtoseconds cannot arise from nondegenerate modes.

For relatively long input pulses (e.g., a 10 ps input pulse carried by 15 modes, see Fig. 2 of Supplementary note 2), groups of modes separate temporally. However, in this case, it is still possible to inject the proper energy in each group of degenerate modes, in order to obtain the generation of several independent spatiotemporal solitons.

Conclusions
MM solitons composed by nondegenerate modes have unique properties of evolving, in the range of hundreds of nonlinearity lengths, into stable single-mode pulses. Their pulsewidth and energy do not depend on the input pulsewidth, but only on the coupling conditions and the input wavelength. Therefore, spatiotemporal solitons composed by nondegenerate modes with pulsewidth larger than a few hundreds of femtoseconds cannot be generated. The unique properties of walk-off solitons can be advantageously used to develop high-power spatiotemporal mode-locked MM fiber lasers, with pulses of fixed duration at a given wavelength. The additional ability to form a single-mode beam can be used for high-energy beam delivery applications.

Methods
Simulations. Numerical simulations are based on a coupled-mode equations approach[25,26], which requires the preliminary knowledge of the input power distribution among fiber modes. The model couples the propagating mode fields via Kerr nonlinearities, by four-wave mixing terms of the type $Q_{plmn}A_lA_mA_n^*$, being Q_{plmn} the coupling coefficients, proportional to the overlap integrals of the transverse modal field distributions, and by SRS with same coupling coefficients. Fiber dispersion and nonlinearity parameters are estimated to be $\beta_2 = -28.8$ ps^{2}km^{-1} at 1550 nm, $\beta_3 = 0.142$ ps^{3}km^{-1}; nonlinear index $n_2 = 2.7 \times 10^{-27}$ m^{2}W^{-1}, Raman response $h_R(t)$ with typical times of 12.2 and 32 fs[27,28]. Wavelength-dependent linear losses of silica were included.

Experiments. The experimental setup included an ultrashort pulse laser system, composed by a hybrid optical parametric amplifier (Lightconversion ORPHEUS-F), pumped by a femtosecond Yb-based laser (Lightconversion PHAROS-SP-HP), generating pulses at 100 kHz repetition rate with Gaussian beam shape ($M^2 = 1.3$); the central wavelength was tunable between 1300 and 1700 nm, and the pulsewidth ranged between 60 and 240 fs, depending on the wavelength and the insertion of pass-band filters. The laser beam was focused by a 50 mm lens into the fiber, with a $1/e^2$ input diameter of ~30 µm (15 µm beam waist). The laser pulse input energy was controlled by means of an external attenuator, and varied between 0.1 and 20 nJ. Care was taken during the input alignment in order to observe, in the linear regime, an output near-field that was composed by axial modes only; this could be particularly appreciated for long lengths of GRIN fiber (120 m and more). The used fiber was a span (from 1 to 850 m) of parabolic GRIN fiber, with core radius $r_c = 25$ µm, cladding radius 62.5 µm, cladding index $n_{clad} = 1.444$ at 1550 nm, and relative index difference $\Delta = 0.0103$. At the fiber output, a micro-lens focused the near field on an InGaAs camera (Hamamatsu C12741-03); a second lens focused the beam into an optical spectrum analyzer (Yokogawa AQ6370D) with wavelength range of 600–1700 nm, and to a real-time multiple octave spectrum analyzer (Fastlite Mozza) with a spectral detection range of 1100–5000 nm. The output pulse temporal shape was inspected by using an infrared fast photodiode, and an oscilloscope (Teledyne Lecroy WavePro 804HD) with 30 ps overall time response, and an intensity autocorrelator (APE pulseCheck 50) with femtosecond resolution.

Data availability

The data that underlie the plots within this paper and other findings of this study are available from the corresponding authors on reasonable request.

Code availability

The code used to generate simulated data and plots is available from the corresponding authors on reasonable request.

References

1. Hasegawa, A. Self-confinement of multimode optical pulse in a glass fiber. *Opt. Lett.* **5**, 416–417 (1980).
2. Crosignani, B. & Porto, P. D. Soliton propagation in multimode optical fibers. *Opt. Lett.* **6**, 329–330 (1981).
3. Grudinin, A. B., Dianov, E., Korbkin, D., Prokhorov, A. M. & Khaidarov, D. Nonlinear mode coupling in multimode optical fibers; excitation of femtosecond-range stimulated-Raman-scattering solitons. *J. Exp. Theor. Phys. Lett.* **47**, 356–359 (1988).
4. Krupa, K. et al. Multimode nonlinear fiber optics, a spatiotemporal avenue. *APL Photonics* **4**, 110901 (2019).
5. Renninger, W. H. & Wise, F. W. Optical solitons in graded-index multimode fibres. *Nat. Commun.* **4**, 1719 (2013).
6. Wright, L. G., Renninger, W. H., Christodoulides, D. N. & Wise, F. W. Spatiotemporal dynamics of multimode optical solitons. *Opt. Express* **23**, 3492–3506 (2015).
7. Zhu, Z., Wright, L. G., Christodoulides, D. N. & Wise, F. W. Observation of multimode solitons in few-mode fiber. *Opt. Lett.* **41**, 4819–4822 (2016).
8. Wright, L. G., Christodoulides, D. N. & Wise, F. W. Controllable spatiotemporal nonlinear effects in multimode fibers. *Nat. Photonics* **9**, 306–310 (2015).
9. Wright, L. G., Wabnitz, S., Christodoulides, D. N. & Wise, F. W. Ultrabroadband dispersive radiation by spatiotemporal oscillation of multimode waves. *Phys. Rev. Lett.* **115**, 223902 (2015).
10. Zitelli, M. et al. High-energy soliton fission dynamics in multimode GRIN fiber. *Opt. Express* **28**, 20473–20488 (2020).
11. Zitelli, M., Ferraro, M., Mangini, F. & Wabnitz, S. Singlemode spatiotemporal soliton attractor in multimode GRIN fibers. *Photonics Res.* **9**, 741–748 (2021).
12. Sidelnikov, O. S., Podivilov, E. V., Fedoruk, M. P. & Wabnitz, S. Random mode coupling assists Kerr beam self-cleaning in a graded-index multimode optical fiber. *Opt. Fiber Technol.* **53**, 101994 (2019).
13. Yu, S.-S., Chien, C.-H., Lai, Y. & Wang, J. Spatio-temporal solitary pulses in graded-index materials with Kerr nonlinearity. *Opt. Commun.* **119**, 167–170 (1995).
14. Raghavan, S. & Agrawal, G. P. Spatiotemporal solitons in inhomogeneous nonlinear media. *Opt. Commun.* **180**, 377–382 (2000).
15. Karlsson, M., Anderson, D. & Desaix, M. Dynamics of self-focusing and self-phase modulation in a parabolic index optical fiber. *Opt. Lett.* **17**, 22–24 (1992).
16. Conforti, M., Mas Arabi, C., Mussot, A. & Kudlinski, A. Fast and accurate modeling of nonlinear pulse propagation in graded-index multimode fibers. *Opt. Lett.* **42**, 4004–4007 (2017).
17. Ahsan, A. S. & Agrawal, G. P. Graded-index solitons in multimode fibers. *Opt. Lett.* **43**, 3345–3348 (2018).
18. Ahsan, A. S. & Agrawal, G. P. Spatio-temporal enhancement of Raman-induced frequency shifts in graded-index multimode fibers. *Opt. Lett.* **44**, 2637–2640 (2019).
19. Terry, N. B., Alley, T. G. & Russell, T. H. An explanation of SRS beam cleanup in graded index fibers and the absence of SRS beam cleanup in step-index fibers. *Opt. Express* **15**, 17509–17519 (2007).
20. Hasegawa, A. & Matsumoto, M. *Optical Solitons in Fibers* (Springer, 2003).
21. Zakharov, V. E. & Wabnitz, S. *Optical Solitons: Theoretical Challenges and Industrial Perspectives* (Springer, 1999).
22. Ho, K. & Kahn, J. Linear propagation effects in mode-division multiplexing systems. *J. Light. Technol.* **32**, 614–628 (2014).
23. Mumtaz, S., Essiambre, R.-J. & Agrawal, G. P. Nonlinear propagation in multimode and multicore fibers: generalization of the Manakov equations. *J. Lightwave Technol.* **31**, 398–406 (2012).
24. Xiao, Y. et al. Theory of intermodal four-wave mixing with random linear mode coupling in few-mode fibers. *Opt. Express* **22**, 32039–32059 (2014).
25. Poletti, F. & Horak, P. Description of ultrashort pulse propagation in multimode optical fibers. *J. Opt. Soc. Am. B* **25**, 1645–1654 (2008).
26. Wright, L. G. et al. Multimode nonlinear fiber optics: massively parallel numerical solver, tutorial, and outlook. *IEEE J. Sel. Top. Quantum Electron.* **24**, 1–16 (2018).
27. Stolen, R. H., Gordon, J. P., Tomlinson, W. J. & Haus, H. A. Raman response function of silica-core fibers. *J. Opt. Soc. Am. B* **6**, 1159–1166 (1989).
28. Agrawal, G. P. *Nonlinear Fiber Optics* 3rd edn (Academic, 2001).

Author contributions

M.Z., F.M. and M.F. carried out the experiments. S.W., M.Z. and O.S. developed the theory and performed the numerical simulations. All authors analyzed the obtained results, and participated in the discussions and in the writing of the manuscript.

Competing interests

The authors declare no competing interests.

Additional information

Supplementary information The online version contains supplementary material available at https://doi.org/10.1038/s42005-021-00687-0.

Correspondence and requests for materials should be addressed to M.Z.

Peer review information *Communications Physics* thanks the anonymous reviewers for their contribution to the peer review of this work. Peer reviewer reports are available.

Reprints and permission information is available at http://www.nature.com/reprints

Publisher's note Springer Nature remains neutral with regard to jurisdictional claims in published maps and institutional affiliations.